haematologica
Journal of the Ferrata Storti Foundation

UBTF tandem duplications in pediatric myelodysplastic syndrome and acute myeloid leukemia: implications for clinical screening and diagnosis

by Juan M. Barajas, Masayuki Umeda, Lisett Contreras, Mahsa Khanlari, Tamara Westover, Michael P. Walsh, Emily Xiong, Chenchen Yang, Brittney Otero, Marc Arribas-Layton, Sherif Abdelhamed, Guangchun Song, Xiaotu Ma, Melvin E. Thomas, Jing Ma, and Jeffery M. Klco

Received: November 15, 2023.
Accepted: February 19, 2024.

Citation: Juan M. Barajas, Masayuki Umeda, Lisett Contreras, Mahsa Khanlari, Tamara Westover, Michael P. Walsh, Emily Xiong, Chenchen Yang, Brittney Otero, Marc Arribas-Layton, Sherif Abdelhamed, Guangchun Song, Xiaotu Ma, Melvin E. Thomas, Jing Ma, and Jeffery M. Klco. UBTF tandem duplications in pediatric myelodysplastic syndrome and acute myeloid leukemia: implications for clinical screening and diagnosis. Haematologica. 2024 Feb 29. doi: 10.3324/haematol.2023.284683 [Epub ahead of print]

Publisher's Disclaimer.
E-publishing ahead of print is increasingly important for the rapid dissemination of science. Haematologica is, therefore, E-publishing PDF files of an early version of manuscripts that have completed a regular peer review and have been accepted for publication. E-publishing of this PDF file has been approved by the authors. After having E-published Ahead of Print, manuscripts will then undergo technical and English editing, typesetting, proof correction and be presented for the authors' final approval; the final version of the manuscript will then appear in a regular issue of the journal. All legal disclaimers that apply to the journal also pertain to this production process.

UBTF tandem duplications in pediatric myelodysplastic syndrome and acute myeloid leukemia: implications for clinical screening and diagnosis

Short Title *UBTF*-TD in pediatric myeloid neoplasms

Authors and Affiliations

Juan M. Barajas[1,+], Masayuki Umeda[1,+], Lisett Contreras[1], Mahsa Khanlari[1], Tamara Westover[1], Michael P. Walsh[1], Emily Xiong[1], Chenchen Yang[2], Brittney Otero[2], Marc Arribas-Layton[2], Sherif Abdelhamed[1], Guangchun Song[1], Xiaotu Ma[3], Melvin E. Thomas 3rd[1], Jing Ma[1], Jeffery M. Klco[1,*]

+ Equal first authors

* Corresponding author

1. Department of Pathology, St. Jude Children's Research Hospital, Memphis, TN, USA.
2. Mission Bio, South San Francisco, CA
3. Department of Computational Biology, St. Jude Children's Research Hospital, Memphis, TN, USA.

Contact Information/Corresponding authors:

*Correspondence: jeffery.klco@stjude.org

Jeffery M. Klco: Mail Stop 342, Room D4047B, St. Jude Children's Research Hospital, 262 Danny Thomas Place, Memphis, TN 38105-3678, Phone: (901) 595-6807, Fax: (901) 595-5947, Email: jeffery.klco@stjude.org

Funding:

The work was funded by the American Lebanese and Syrian Associated Charities of St. Jude Children's Research Hospital, the Jane Coffin Childs Fund (JMB) and funds from the US NIH, including F32 HL154636 (JMB), U54 CA243124 and R01 CA276079 (JMK). The content, however, does not necessarily represent the official views of the NIH and is solely the responsibility of the authors. JMK holds a Career Award for Medical Scientists from the Burroughs Welcome Fund. Support was also provided by Shared Resources provided through the St. Jude Comprehensive Cancer Center (P30-CA21765), including Flow Cytometry and Cell Sorting, Comparative Pathology Core, and Genome Sequencing (Hartwell Center).

Author Contributions:

Contributions: Conceptualization, J.M.K; Methodology, J.M.B., L.C., E.X.; Software, Validation, J.M.B., L.C., E.X.; Formal Analysis, J.M.B., M.U., B.O., M.A.L., M.K.; Investigation, J.M.B., M.U., L.C., M.P.W., M.K., M.E.T., X.M.; Resources, J.M.K.; Data Curation, T.W., G.S.; Writing – Original Draft, J.M.B., M.U.; Writing – Review & Editing, all authors were involved in review & editing of the manuscript; Visualization, J.M.B., M.U.; Supervision, J.M.K., Project Administration, J.M.B., M.U., T.W., S.A., J.M.K.; Funding Acquisition, J.M.B., J.M.K.

Competing Interests: C.Y., B.O., and M.A. are employed by Mission Bio, Inc. No other authors have conflicts to declare.

Data Availability Statement:

The expression data newly generated in this study (RNA-sequencing: n=3) and scDNA + protein sequencing (n=3) have been deposited in the European Genome-Phenome Archive (EGA) which is hosted by the European Bioinformatics Institute (EBI), under accession EGAS00001005760. The remaining RNA-sequencing data are available via EGA, St. Jude Cloud or TARGET/GDC as defined in **Supplemental Table 1**. Information about TARGET can be found at http://ocg.cancer.gov/programs/target. Other data generated in this study are available in the Supplemental tables or upon request to the corresponding author.

Word Count (includes Methods/Introduction/Results/Discussion): 3,090/4,500

Figures: 5/7

Abstract, (199/200 words):

Recent genomic studies in adult and pediatric acute myeloid leukemia (AML) demonstrated recurrent in-frame tandem duplications (TD) in exon 13 of upstream binding transcription factor (*UBTF*). These alterations, which account for ~4.3% of AMLs in childhood and about 3% in adult AMLs under 60, are subtype-defining and associated with poor outcomes. Here, we provide a comprehensive investigation into the clinicopathological features of *UBTF*-TD myeloid neoplasms in childhood, including 89 unique pediatric AML and 6 myelodysplastic syndrome (MDS) cases harboring a tandem duplication in exon 13 of *UBTF*. We demonstrate that *UBTF*-TD myeloid tumors are associated with dysplastic features, low bone marrow blast infiltration, and low white blood cell count. Furthermore, using bulk and single-cell analyses, we confirm that *UBTF*-TD is an early and clonal event associated with a distinct transcriptional profile, whereas the acquisition of *FLT3* or *WT1* mutations is associated with more stem cell-like programs. Lastly, we report rare duplications within exon 9 of *UBTF* that phenocopy exon 13 duplications, expanding the spectrum of *UBTF* alterations in pediatric myeloid tumors. Collectively, we comprehensively characterize pediatric AML and MDS with *UBTF*-TD and highlight key clinical and pathologic features that distinguish this new entity from other molecular subtypes of AML.

Key Words:

UBTF Tandem Duplications; Pediatric and Adult Acute Myeloid Leukemia; Myeloid Neoplasms

Introduction:

Pediatric acute myeloid leukemia (AML) and myelodysplastic syndrome (MDS) are characterized by unique genetic backgrounds when compared to those in adults (1-3). Recurrent tandem duplications (TD) of exon 13 of upstream binding transcription factor (*UBTF*) were only recently identified as potential initiating events in pediatric AML (4-7), accounting for about 4% of newly diagnosed pediatric AML. PCR-based screening covering exon 13 of *UBTF* also identified *UBTF*-TD alterations in large adult AML cohorts (8, 9). These studies significantly contributed to the accumulation of evidence of *UBTF*-TD alterations in adult AML. However, PCR-based methods potentially underestimate partial tandem duplications (PTD) extending outside the regions covered by amplicons or possible alterations not involving exon 13 (9). Also, data on *UBTF* alterations in pediatric AML is limited to screening of relatively small cohorts (4, 5), and further efforts are needed to accumulate more knowledge about the biology and clinicopathologic features of this disease entity.

UBTF encodes for the UBTF/UBF protein that regulates ribosomal RNA (rRNA) transcription and nucleolar formation (10, 11). We previously reported that expression of exon 13 UBTF-TD in cord blood CD34+ (cbCD34+) cells is sufficient to induce cellular proliferation, increase clonogenic activity, and it establishes a transcriptional signature that recapitulates what is observed in UBTF-TD AML patient samples. (4). Our previous analyses also demonstrated that *UBTF*-TDs do not occur with other canonical alterations in pediatric AML, but that *UBTF*-TD AMLs often harbor additional somatic mutations, such as internal tandem duplications in *FLT3* (*FLT3*-ITD) and frameshift

mutations in *WT1*. The acquisition of these cooperating mutations can likely contribute to the stepwise progression of the disease and clonal evolution. However, our understanding of how these cooperating mutations contribute to the cellular and disease status remains to be elucidated.

To bridge these knowledge gaps, we present an extended pediatric and young adult cohort of 89 AML and 6 MDS samples with exon 13 *UBTF*-TD, showing that *UBTF*-TD neoplasms are strongly associated with dysplastic features and unique patterns of cooperating mutations. By leveraging bulk RNA-sequencing (RNA-seq) and single cell proteogenomics, we show that the co-occurrence of *FLT3*-ITD and *WT1* mutations is associated with stem cell-like phenotypes. Furthermore, we identified tandem duplications within exon 9 of *UBTF* in two cases transcriptionally resembling exon 13 *UBTF*-TD AML. Exon 9 UBTF-TDs contain analogous hydrophobic leucine-rich sequences as the exon 13 duplications and similarly induce leukemic phenotypes in cbCD34+ cells, suggesting that they likely have a shared mechanism and should be classified as the same molecular entity. These findings offer valuable insights to inform future diagnostic strategies and understanding of the molecular basis of *UBTF*-TD myeloid neoplasms.

Methods (435/500):

Single-Cell DNA Sequencing and Analysis

Single-cell targeted sequencing was performed using Tapestri System from Mission Bio (missionbio.com). A panel consisting of 162 PCR amplicons targeting genes commonly mutated in pediatric AML with an average size of 260bp was designed using Tapestri Designer from Mission Bio (designer.missionbio.com), as well as a manually designed amplicon targeting the *UBTF* exon13 TD region (**Supplemental Table 2**). Cryopreserved *UBTF*-TD primary AML samples were thawed and subjected to dead cell removal using the EasySep™ Dead Cell Removal Kit (STEMCELL Technologies, cat# 17899). Live cells were then subjected to the Mission Bio DNA+Protein (TotalSeq™-D Heme Oncology Protein Panel) protocol per manufacturer's instructions (missionbio.com). Libraries were sequenced on the Novaseq platform (100M read pairs for DNA libraries and 225M read pairs for protein libraries). BAM files, loom files, h5 files, and QC metrics were produced via a customization of the Tapestri pipeline developed by Mission Bio (support.missionbio.com/hc/en-us). Analysis of the samples was completed using the Mosaic package v3.0.1 (missionbio.github.io/mosaic/). Reads for the *UBTF*-TD and *FLT3*-ITD calls were isolated from bam files using the pysam python package v0.21.0 (github.com/pysam-developers/pysam). Reads were then realigned to ITD contigs reported in previous studies (4) using the BWA aligner v0.7.15-r1140 (12, 13). When necessary, mutation variant allele frequencies (VAFs) were adjusted using pysam.

Transcriptome analysis

Gene expression analysis was performed as previously described (1). Briefly, an RNA-seq cohort was established by integrating *UBTF*-TD cases with RNA-seq data in this

study (n=96) and AML in other categories (n=837) and cbCD34+ cells (n=5) (1). Reads from aligned RNA-seq BAM files were assigned to genes and counted using HTSeq (v0.11.2) (14) with the GENCODE human release 19 gene annotation. The count data were transformed to log2-counts per million (log2CPM) using Voom available from R package Limma (v3.50.3) (15). The top variable genes were selected using the "vst" method in Seurat package (16). The expression data were then scaled, and PCA (Principal Component Analysis) was performed on the scaled data using the top 265 variable genes. Dimension reduction was performed using UMAP (Uniform Manifold Approximation and Projection) (17) with the top 100 principal components. Differential gene expression analysis was performed by Limma between groups as indicated in each figure, and we set Log2 CPM = -1 if it is < -1 based on the Log2 CPM data distribution. *P* values were adjusted by the Benjamini-Hochberg method to calculate the false discovery rate (FDR) using R function p.adjust. Genes with absolute fold change > 2 and FDR < 0.05 were regarded as significantly differentially expressed. Gene Set Enrichment Analysis (GSEA) was performed by GSEA (v4.2.3) using MSigDB gene sets c2.all (v7.5.1) (18). Permutations were done 1000 times among gene sets with sizes between 15 and 1500 genes.

IRB Approval and Ethics Committee

Samples from patients with MDS or AML from St. Jude Children's Research Hospital tissue resource core facility were obtained with written informed consent using a protocol approved by the St. Jude Children's Research Hospital institutional review

board (IRB). Studies were conducted in accordance with the International Ethical Guidelines for Biomedical Research Involving Human Subjects.

Statistics

Details about statistical comparisons are provided in each figure legend. All the computations were done using R or GraphPad Prism, and all *P* values are 2-sided.

Results:

UBTF-TD in pediatric myeloid neoplasms.

Our previous study described the molecular features of 27 pediatric AML cases with exon 13 *UBFT*-TD (4). To expand the cohort and better understand the biology, we screened RNA-seq data from pediatric and young adult MDS and AML samples and identified an additional 68 cases from available datasets and previously published studies (2, 19) and routine clinical service at St. Jude Children's Research Hospital. All 95 cases (median age = 14.0 yrs., range = 2.4-27.4, **Supplemental Figure 1A**) possessed exon 13 *UBTF*-TDs encoding a consensus hydrophobic leucine-rich ELTRLLARM amino acid motif within the duplications (**Figure 1A, Supplemental Table 3**). The duplications resulted in an increased size of exon 13 (median size = 60 bp, range = 45-339 bp) (**Figure 1B**). Consistent with previous findings, *UBTF*-TD did not co-occur with other subtype-defining alterations and showed high VAFs (median = 36.3%, range = 13.5-78.1%), further supporting our previous assertion that *UBTF*-TD alterations are early clonal events (1, 4) (**Figure 1C**). We further investigated the mutational background of this *UBTF*-TD cohort, confirming a strong association with a normal karyotype or trisomy 8 (**Supplemental Figure 1B-C**), as well as with *FLT3*-ITD

(n=55, 57.9%) and mutations in *WT1* (n=39, 41.1%), which are highly co-occurring (**Supplemental Figure 1D**, *P*=0.011, Fisher's exact test) with 30.1% (n=29) cases harboring both alterations. In addition, 26.6% (n=25) of cases also had at least one mutation in Ras-MAPK pathway genes: *NRAS* (n=17,17.9%); *PTPN11* (n=5, 5.3%); *RIT1* (n=5, 5.3%); *NF1* (n=4, 4.2%); *CBL* (n=2, 2.1%); and *KRAS* (n=2, 2.1%). Other recurrent mutations in myeloid malignancies were rarely observed, including *IDH1*/*IDH2* (n=3, 3.2%), *BCOR* (n=2, 2.1%), and *RUNX1* (n=1, 1.1%). We also screened MDS cases and identified *UBTF*-TD in 6 cases of pediatric MDS, all with normal karyotype. These include 3 primary pediatric MDS cases from our previously published cohort (2), classified as childhood MDS with increased blasts according to the current WHO classification (20). These three cases lacked a known germline predisposition (e.g. *GATA2*, *SAMD9*, *SAMD9L*) and had normal bone marrow cytogenetics. Collectively, *UBTF*-TD was present in 3/38 (7.9%) of the primary MDS cases without a known germline predisposition, as well as 3/22 (13.6%) of all cases of childhood MDS with increased blasts. No *FLT3*-ITD mutations were detected in the 6 MDS cases, while *WT1* mutations were present in 3 out of the 6 MDS cases, suggesting clonal evolutionary patterns initiating with *UBTF*-TD alterations.

To address clonal evolution in *UBTF*-TD myeloid neoplasms, we utilized a droplet-based single cell proteogenomic platform from MissionBio (**Figure 2**) (21). This platform enables the concurrent detection of *UBTF*-TD alterations and somatic mutations by a custom-targeted DNA panel and cell classification using DNA-oligo conjugated antibodies targeting cell surface markers at the single cell level. In a single timepoint

AML case, we found a clonal *UBTF*-TD alteration. A small fraction of the cells only contained the *UBTF*-TD alteration, whereas the major population also contained a *WT1* (*p*.V359fs) mutation (**Supplemental Table 4, Figure 2A-B**). Distinct *UBTF*-TD+*WT1*+ minor subclones defined by *NRAS* (*p*.G12D) or *FLT3* (*p*.V592D) were also present, representing branched evolution of the *UBTF*-TD+*WT1*+ clone. We also found that cells with $WT1^{+}FLT3^{+}$ mutations were associated with high stem cell marker protein expression (CD34, CD117, or CD123) compared with the *UBTF*-TD-only population, whereas the $WT1^{+}NRAS^{+}$ population was characterized by low expression of these markers. In a diagnosis and relapse-paired case, we found that the identical *UBTF*-TD was retained through disease progression along with an *FLT3*-ITD alteration (**Figure 2C-D**). Interestingly, a minor $WT1^{+}$ (*p.*R375fs) subclone at diagnosis was eradicated after chemotherapy, whereas a different $WT1^{+}$ (*p.*R353fs) clone became dominant at relapse, showing high expression of CD34, CD117, and CD123. These data collectively confirm that *UBTF*-TD is an early initiating event, while somatic mutations are subclonal to *UBTF*-TD, possibly contributing to disease progression toward subclones with unique expression profiles.

Clinical features of UBTF-TD pediatric myeloid neoplasms

UBTF-TD AML showed a variety of morphologic features associated with cellular differentiation, as evidenced by variable FAB (French-American-British) classifications (**Figure 3A, Supplemental Table 5**). Although AML with maturation (FAB M2) was the most common (19/43, 44.2%), cases with erythroid features, including FAB M6 (6/43, 14.0%), were also observed, as was also recently described for *UBTF*-TD AMLs in

adults (9). Morphologic assessments also revealed that *UBTF*-TD cases often displayed pleomorphic blasts (**Figure 3B**), accompanied by background multilineage dysplasia and increased erythroid precursors. *UBTF*-TD AMLs showed lower white blood cell count (median = $10.0x10^9$/L, range = $0.6\text{-}409.4x10^9$/L) and bone marrow blast percentage (median = 39.5%, range = 2-97%) when compared to other AMLs, including those with similar transcriptional profiles like AML with *NUP98*-rearrangements or *NPM1* mutations (1, 4) (**Figure 3C-D**). *FLT3*-ITD, but not *WT1* mutations, were associated with a higher white blood cell count (WBC) count and bone marrow blasts in *UBTF*-TD AMLs (**Figure 3E**). Despite the presence of dysplastic features, cytogenetic studies commonly found either a normal karyotype (58/92, 63.0%) or trisomy 8 (27/92 29.3%). Myelodysplasia-related chromosomal changes or myelodysplasia-related mutations were overall rare, suggesting that *UBTF*-TD itself contributes to dysplastic features (**Supplemental Table 5**). Considering these overall features and other recent publications (5, 8, 9, 22, 23), the majority of *UBTF*-TD AMLs (83/89, 93.3%) are best classified as "Acute myeloid leukemia with other defined genetic alterations" in the current WHO classification (20) (**Supplemental Table 5**).

Transcriptional features of UBTF-TD myeloid neoplasms

We and others have previously shown that AML with *UBTF*-TD is characterized by high *HOXA* and *HOXB* cluster gene expression, similar to *NPM1*-mutated or *NUP98*::*NSD1* AML (1, 8). To further define the unique expression profiles of *UBTF*-TD, we established an RNA-seq cohort consisting of various AML subtypes (1) (n=837), cord blood CD34+ samples from healthy donors (n=5), and *UBTF*-TD AML and MDS samples (n=94: 1

UBTF-TD case did not have RNA-seq data available) (**Figure 4A**). Consistent with previous data, *UBTF*-TD cases clustered with *NPM1*-mutated and *NUP98::NSD1* AMLs. However, *UBTF*-TD samples displayed a significantly higher expression of a subset of *HOXB* cluster genes (e.g., *HOXB8, HOXB9*) compared with *NUP98*::*NSD1* AML (**Supplemental Figure 2A**). We also observed uniquely high expression of histone genes (e.g., *HIST1H4F* and *HIST1H1D*) compared to *NPM1*-mutated AML (**Supplemental Figure 2B**), suggesting transcriptional mechanisms unique to *UBTF*-TD AML. Within *UBTF*-TD samples, those with *FLT3*-ITD and *WT1* mutations showed unique distribution on the UMAP cluster (**Supplemental Figure 2C**), and each mutation group demonstrated differential gene expression against *UBTF*-TD samples without either mutation (**Figure 4B**). Co-occurrence of *WT1* and *FLT3*-ITD was associated with stemness-related genes (e.g., *CD34* and *DNTT,* **Supplemental Figure 2D**), and Gene Set Enrichment Analysis (GSEA) confirmed enrichment of stemness or cell cycle-related gene expression in *WT1*$^{+}$*FLT3*-ITD^{+} *UBTF*-TD samples (**Figure 4C**). These results show the unique expression profile of *UBTF*-TD AML and the specific influence of additional cooperating mutations, which can likely impact patterns of clonal evolution.

Exon 9 tandem duplications in UBTF

Given the recurrent *UBTF* exon 13 alterations duplicating specific hydrophobic amino acid sequences, we hypothesized that *UBTF* alterations outside exon 13 resulting in similar amino acid sequences could be found in cases without defining alterations but with a similar expression signature. By close inspection of the *UBTF* gene using RNA-seq data, we found two pediatric AML cases without exon 13 *UBTF*-TD or other driver

alterations that instead have in-frame tandem duplications (lengths of 78 and 153bp) in exon 9 of *UBTF* (TD-exon9), encoding short hydrophobic amino acid sequences (**Figure 5A-B**). These cases express *HOXA/B* cluster genes comparably to exon 13 *UBTF*-TD (**Supplemental Figure 3**), and one had a *WT1* mutation (**Supplemental Table 6**). To test whether UBTF-TD-exon9 alterations could lead to cellular transformation, we expressed both UBTF-TD-exon9 in cbCD34+ cells using lentiviral vectors and assessed their impact on cell proliferation, clonogenic potential, and cellular morphology in comparison with control conditions and exon 13 UBTF-TD (**Figure 5C-D**). Colony-forming unit (CFU) assay revealed that the expression of both UBTF-TD-exon9 increased the total colony number (**Figure 5E**). After the second round of replating, cells with UBTF-TD-exon9 showed an immature morphology along with erythroid features, similar to exon 13 UBTF-TD expressing cells in contrast to control conditions which displayed myeloid differentiation (**Figure 5F**). Furthermore, cells expressing UBTF-TD-exon9 as well as UBTF-TD-exon13 showed a proliferative advantage compared to UBTF-WT and vector controls (**Figure 5G**). Collectively, these data highlight a tandem duplication in *UBTF* exon 9 as a defining alteration functionally equivalent to exon 13 tandem duplications.

Discussion:

In this study we extended our cohort of pediatric myeloid malignancies with exon 13 *UBTF*-TD, which now includes 95 pediatric and young adult cases. Similar to studies in adults (9), pediatric myeloid tumors with *UBTF*-TD have a lower bone marrow blast infiltration and lower peripheral white blood cell count, suggesting a continuum of a

common entity across the age spectrum. We observed that *UBTF*-TD neoplasms showed variable cellular morphology and differentiation, including FAB M2 (44.2%), but also cases with erythroid features. These morphological features align with findings in adult cases, which showed a high prevalence of FAB M6 and M2 cases (9). Furthermore, the presence of dysplastic features and the observation that *UBTF*-TD occurs in cases of pediatric MDS suggest that MDS and AML could be part of a continuum driven by *UBTF*-TD. These findings are consistent with the recognition of *UBTF*-TD alterations in nearly a third of pediatric patients with high-grade MDS (24) and recent studies have also identified the persistence of *UBTF*-TD in remission samples in patients with UBTF-TD myeloid neoplasms (22). These collective data support the conclusion that UBTF-TD alterations can lead to both MDS and AML and that *UBTF*-TD myeloid neoplasms should be recognized as a separate entity.

Our data also suggest that progression to AML may be promoted by the acquisition of cooperating mutations, such as *FLT3*-ITD. This is supported by the finding that none of the MDS cases in this cohort harbored a *FLT3*-ITD alteration, although this may be limited by the small size of the MDS cohort (n=6) in this study. However, the lack of *FLT3* or RAS pathway variants in a subset of AML cases suggest that *UBTF*-TD could be sufficient for leukemic transformation in some cases. Our analyses, including single cell studies, also showed that the co-occurrence of *FLT3*-ITD and *WT1* is strongly associated with progressive stem cell features as represented by CD34 expression or quiescent states. Thus, the patterns of mutational cooperativity likey will influence disease phenotypes.

Given that exon 13 *UBTF*-TD has been underappreciated in AML studies using standard computational pipelines, we investigated other possible *UBTF* alterations in pediatric AML cases without a defined driver event and demonstrated that in-frame tandem duplications in exon 9 of *UBTF* are additional possible driver alterations. Although rare within cases with *UBTF* alterations (2/97 *UBTF*-TD cases, 2.1%), cases with tandem duplications in exon 9 show similar transcriptional profiles to exon 13 *UBTF*-TD AML. We further show that exon 9 alterations can induce leukemic changes, including hematopoietic cell growth and increased clonogenicity in cbCD34+ cells similar to exon 13 alterations. At the amino acid level, exon 9 tandem duplications contain hydrophobic amino acid sequences (LKDKFDGL) that are similar to the sequences in exon 13 tandem duplications (LTRLLARM), suggesting a shared mechanism. Importantly, PCR-based exon 13 screening could potentially underestimate PTD involving exon 13 and flanking regions or these exon 9 alterations (9), and we propose unbiased sequencing-based strategies to diagnose this entity accurately. The findings presented here will help build on our understanding of *UBTF*-TD myeloid neoplasms and further support its recognition as a distinct entity in future classification systems.

References

1. Umeda M, Ma J, Westover T, et al. A new genomic framework to categorize pediatric acute myeloid leukemia. Nat Genet. 2024;56(2):281-293.

2. Schwartz JR, Ma J, Lamprecht T, et al. The genomic landscape of pediatric myelodysplastic syndromes. Nat Commun. 2017;8(1):1557.

3. Bolouri H, Farrar JE, Triche T, Jr., et al. The molecular landscape of pediatric acute myeloid leukemia reveals recurrent structural alterations and age-specific mutational interactions. Nat Med. 2018;24(1):103-112.

4. Umeda M, Ma J, Huang BJ, et al. Integrated genomic analysis identifies UBTF tandem duplications as a recurrent lesion in pediatric acute myeloid leukemia. Blood Cancer Discov. 2022;3(3):194-207.

5. Kaburagi T, Shiba N, Yamato G, et al. UBTF-Internal tandem duplication as a novel poor prognostic factor in pediatric acute myeloid leukemia. Genes Chromosomes Cancer. 2022;62(4):202-209.

6. Stratmann S, Yones SA, Mayrhofer M, et al. Genomic characterization of relapsed acute myeloid leukemia reveals novel putative therapeutic targets. Blood Adv. 2021;5(3):900-912.

7. Ma X, Liu Y, Liu Y, et al. Pan-cancer genome and transcriptome analyses of 1,699 paediatric leukaemias and solid tumours. Nature. 2018;555(7696):371-376.

8. Georgi JA, Stasik S, Eckardt JN, et al. UBTF tandem duplications are rare but recurrent alterations in adult AML and associated with younger age, myelodysplasia, and inferior outcome. Blood Cancer J. 2023;13(1):88.

9. Duployez N, Vasseur L, Kim R, et al. UBTF tandem duplications define a distinct subtype of adult de novo acute myeloid leukemia. Leukemia. 2023;37(6):1245-1253.

10. Sanij E, Hannan RD. The role of UBF in regulating the structure and dynamics of transcriptionally active rDNA chromatin. Epigenetics. 2009;4(6):374-382.

11. Moss T, Mars JC, Tremblay MG, et al. The chromatin landscape of the ribosomal RNA genes in mouse and human. Chromosome Res. 2019;27(1-2):31-40.

12. Li H, Durbin R. Fast and accurate long-read alignment with Burrows-Wheeler transform. Bioinformatics. 2010;26(5):589-595.

13. Li H, Handsaker B, Wysoker A, et al. The Sequence Alignment/Map format and SAMtools. Bioinformatics. 2009;25(16):2078-2079.

14. Anders S, Pyl PT, Huber W. HTSeq--a Python framework to work with high-throughput sequencing data. Bioinformatics. 2015;31(2):166-169.

15. Ritchie ME, Phipson B, Wu D, et al. limma powers differential expression analyses for RNA-sequencing and microarray studies. Nucleic Acids Res. 2015;43(7):e47.

16. Satija R, Farrell JA, Gennert D, et al. Spatial reconstruction of single-cell gene expression data. Nat Biotechnol. 2015;33(5):495-502.

17. Becht E, McInnes L, Healy J, et al. Dimensionality reduction for visualizing single-cell data using UMAP. Nat Biotechnol. 2018 Dec 3. [Epub ahead of Print]

18. Subramanian A, Tamayo P, Mootha VK, et al. Gene set enrichment analysis: a knowledge-based approach for interpreting genome-wide expression profiles. Proc Natl Acad Sci U S A. 2005;102(43):15545-15550.

19. Fornerod M, Ma J, Noort S, et al. Integrative Genomic Analysis of Pediatric Myeloid-Related Acute Leukemias Identifies Novel Subtypes and Prognostic Indicators. Blood Cancer Discov. 2021;2(6):586-599.

20. Khoury JD, Solary E, Abla O, et al. The 5th edition of the World Health Organization Classification of Haematolymphoid Tumours: Myeloid and Histiocytic/Dendritic Neoplasms. Leukemia. 2022;36(7):1703-1719.

21. Miles LA, Bowman RL, Merlinsky TR, et al. Single-cell mutation analysis of clonal evolution in myeloid malignancies. Nature. 2020;587(7834):477-482.

22. Harrop S, Nguyen PC, Byrne D, et al. Persistence of UBTF tandem duplications in remission in acute myeloid leukaemia. EJHaem. 2023;4(4):1105-1109.

23. Barajas JM, Rasouli M, Umeda M, et al. Acute myeloid leukemias with UBTF tandem duplications are sensitive to Menin inhibitors. Blood. 2024;143(7):619-630.

24. Erlacher M, Stasik S, Yoshimi A, et al. UBTF tandem Duplications Account for a Third of Advanced Pediatric MDS without Genetic Predisposition to Myeloid Neoplasia. Blood. 2022;140(Supplement 1):1355-1356.

Figure Legends:

Figure 1. Characterization of Tandem Duplications in Exon 13 of *UBTF*. **A**. Genomic representation of duplicated regions (grey) from 95 cases with *UBTF* exon 13 duplications. A common duplicated region is outlined in red with the alignment of the resulting amino acid sequence. **B**. Size assessment of exon 13 resulting from the duplicated regions and associated insertion/deletions. For partial tandem duplications (n=13) extending beyond exon 13, sizes of duplicated exon 13 with insertions or deletions are included. **C**. Genomic landscape of *UBTF*-TD cases. Each column represents an individual patient. For each case, variant allele frequency (VAF), diagnosis, karyotype, and sex are shown.

Figure 2. Clonal Dynamics of *UBTF*-TD Leukemias. **A.** Single-cell DNA sequencing coupled with surface marker expression of *UBTF*-TD case at diagnosis. Heatmap depicting the presence of mutant allele (bottom) and relative protein abundance (top). **B.** Schematic of clonal structure in *UBTF*-TD case from A**.** Percentages are calculated as a proportion of total cells with a somatic mutation. **C.** Single-cell DNA sequencing of a *UBTF*-TD case with diagnosis (left) and relapse (right) paired samples. Heatmap depicts the presence of a mutant allele and protein expression. **D.** Schematic of clonal dynamics in diagnosis/relapse case from C**.** Percentages are calculated as a proportion of total cells with a somatic mutation.

Figure 3. Morphological and Biological Assessment of *UBTF*-TD myeloid neoplasms. A. Available FAB (French-American-British) classification of *UBTF*-TD AMLs (n=43). **B**. Representative Wright-Giemsa Staining of bone marrow (BM) aspirates and peripheral blood (PB) smears from 4 unique *UBTF*-TD cases. Case IDs are labeled above. **SJMDS031973-Childhood MDS with increased blasts**: increased erythroid cells with dysplastic morphologic features (top), dysplastic myeloid cells with salmon-colored granules, and dysplastic small

megakaryocytes (bottom). **SJAML033350-AML with other defined genetic alterations**: characteristic blasts and myeloid precursor cells with salmon-colored granules (top) and blasts with small Auer rods (bottom). **SJAML010730-AML with other defined genetic alterations**: blasts with both myeloid and monocytic/monoblastic morphologic features. PB in this patient is one of the few cases in our cohort showing hyperleukocytosis with many circulating blasts (bottom). **SJAML015028-AML with other defined genetic alterations**: dysplastic megakaryocytes, increased erythroid cells with dysplastic morphologic features, and blasts, many with monocytic/monoblastic morphologic features**. C.** Bone marrow blast percentage for a pediatric AML cohort stratified by oncogenic driver subtypes. **D.** White blood cell counts (WBC) for a pediatric AML cohort stratified by oncogenic driver subtypes. **E.** WBC count and BM blast percentage among *UBTF*-TD cases with different *WT1* and *FLT3* mutation status.

Figure 4. Transcriptional characterization of *UBTF*-TD leukemias. A. UMAP (Uniform Manifold Approximation and Projection) of expression profiles across a cohort of *UBTF*-TD (n=94) and pediatric AML (n=837), adapted from a previous study (1, 4). Each dot is colored by subtype-defining alterations. The black box outlines a cluster of cases with *HOXA/HOXB* dysregulation, which includes all *UBTF*-TD cases. **B-top.** Schematic depicting the transcriptional comparison of *UBTF*-TD cases by mutational status. **-bottom.** Venn diagram showing overlap of differentially expressed genes in *FLT3*-ITD only cases and *FLT3*-ITD+/*WT1*+ cases compared with cases without these mutations. **C.** GSEA of *UBTF*-TD cases based on mutational status.

Figure 5. Exon 9 *UBTF* Tandem Duplications in Pediatric AML. A. Identification of *UBTF*-TD cases with tandem duplications in exon 9 of *UBTF. UBTF*-TD-exon9 on the UMAP plot of the Pediatric AML cohort (red circles), adapted from a previous study (1, 4). **B.** Schematic of UBTF protein, highlighting amino acid sequences encoded in exon 9 of *UBTF*-WT, *UBTF*-TD78-exon9,

UBTF-TD153-exon9. Duplications resulting in short hydrophobic sequences are labeled in red. Hydrophobic residues are underlined. **C.** Experimental design to evaluate the transforming potential of UBTF-TD-exon9 mutants **D.** Immunoblot of lysates from cbCD34+ cells transduced with UBTF-TD-exon9 vectors and corresponding controls. Antibodies against HA-tag, UBTF, and β-actin were used. **E**. Colony forming unit assay. 2-way ANOVA with two-sided Dunnett's test was applied with UBTF-WT as control **F.** Cytospins isolated from CFU assay at round 2 of replating (Wright-Giemsa Staining, 400X magnification). **G.** In vitro growth curves of cbCD34+ cells expressing controls or UBTF-TD-e9 mutants. 2-way ANOVA with Dunnett's test was applied with UBTF-WT as control.

Figure 1

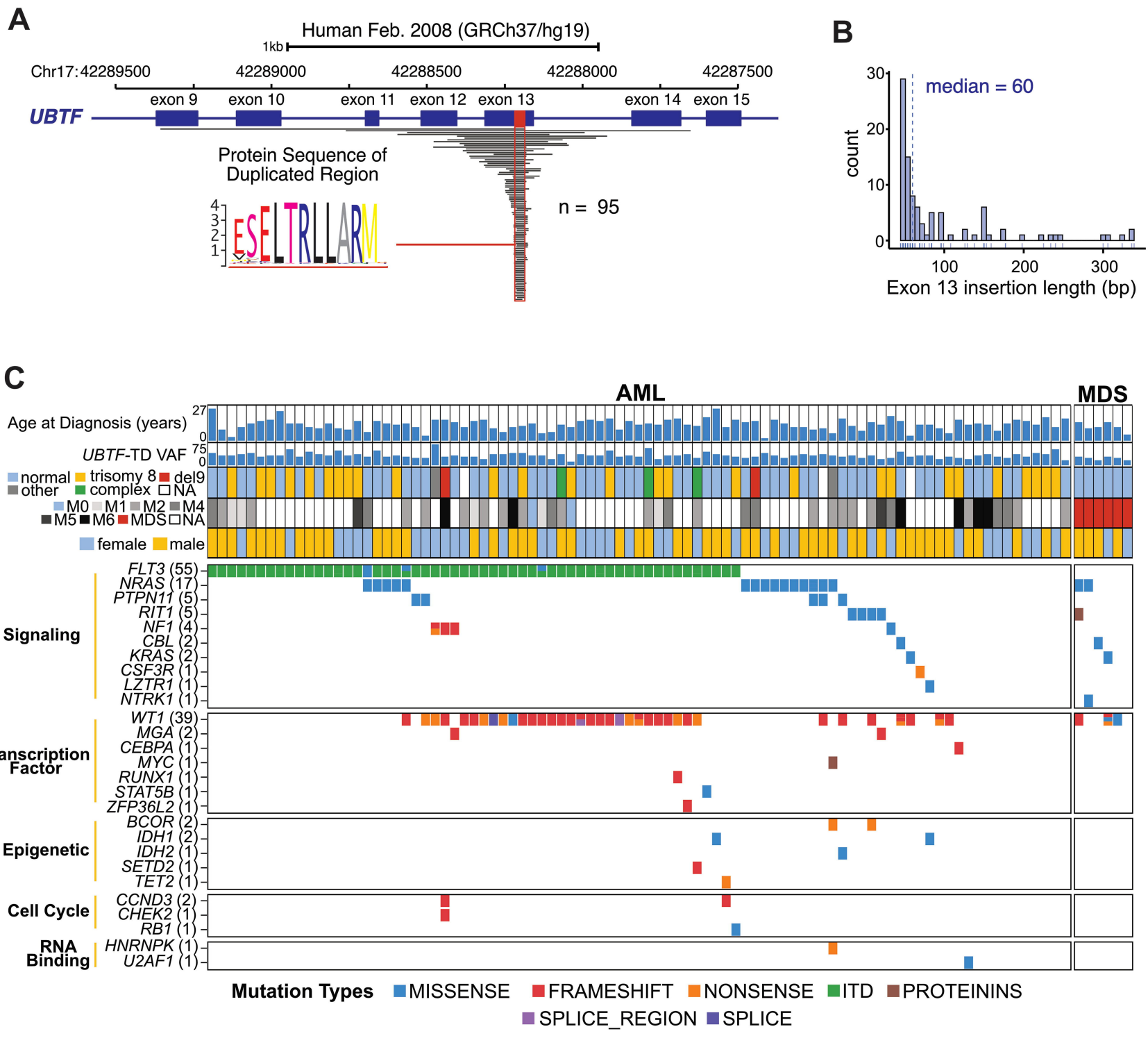
A
Human Feb. 2008 (GRCh37/hg19)
1kb
Chr17:42289500
42289000
42288500
42288000
42287500
exon 9
exon 10
exon 11
exon 12
exon 13
exon 14
exon 15
UBTF
Protein Sequence of Duplicated Region
n = 95
B
median = 60
count
Exon 13 insertion length (bp)
C
AML
MDS
Age at Diagnosis (years)
UBTF-TD VAF
normal
trisomy 8
del9
other
complex
NA
M0
M1
M2
M4
M5
M6
MDS
female
male
Signaling
FLT3 (55)
NRAS (17)
PTPN11 (5)
RIT1 (5)
NF1 (4)
CBL (2)
KRAS (2)
CSF3R (1)
LZTR1 (1)
NTRK1 (1)
Transcription Factor
WT1 (39)
MGA (2)
CEBPA (1)
MYC (1)
RUNX1 (1)
STAT5B (1)
ZFP36L2 (1)
Epigenetic
BCOR (2)
IDH1 (2)
IDH2 (1)
SETD2 (1)
TET2 (1)
Cell Cycle
CCND3 (2)
CHEK2 (1)
RB1 (1)
RNA Binding
HNRNPK (1)
U2AF1 (1)
Mutation Types
MISSENSE
FRAMESHIFT
NONSENSE
ITD
PROTEININS
SPLICE_REGION
SPLICE

Figure 2

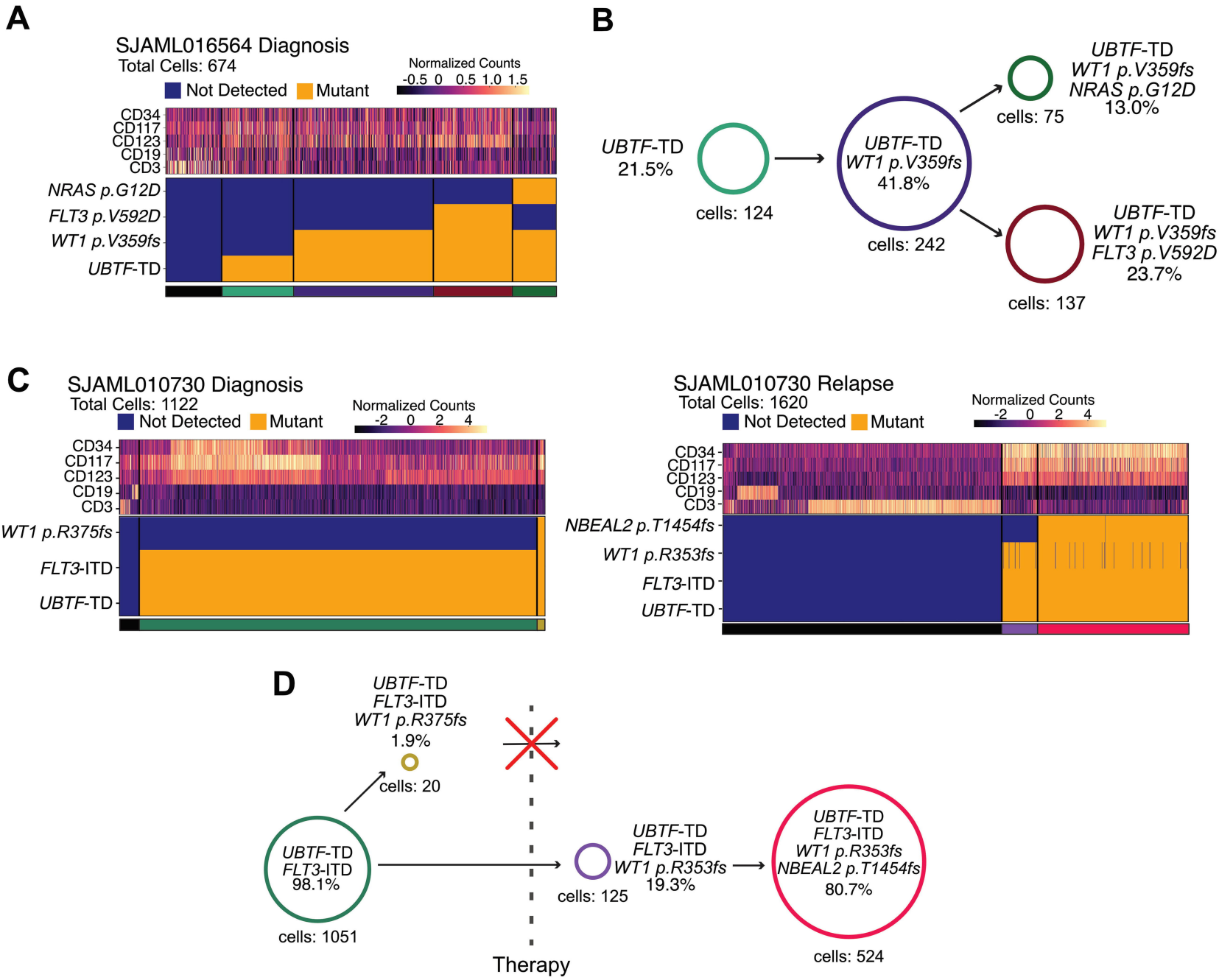
A
SJAML016564 Diagnosis
Total Cells: 674
Not Detected
Mutant
Normalized Counts
-0.5 0 0.5 1.0 1.5
CD34
CD117
CD123
CD19
CD3
NRAS p.G12D
FLT3 p.V592D
WT1 p.V359fs
UBTF-TD
B
UBTF-TD
21.5%
cells: 124
UBTF-TD
WT1 p.V359fs
41.8%
cells: 242
UBTF-TD
WT1 p.V359fs
NRAS p.G12D
13.0%
cells: 75
UBTF-TD
WT1 p.V359fs
FLT3 p.V592D
23.7%
cells: 137
C
SJAML010730 Diagnosis
Total Cells: 1122
Not Detected
Mutant
Normalized Counts
-2 0 2 4
CD34
CD117
CD123
CD19
CD3
WT1 p.R375fs
FLT3-ITD
UBTF-TD
SJAML010730 Relapse
Total Cells: 1620
Not Detected
Mutant
Normalized Counts
-2 0 2 4
CD34
CD117
CD123
CD19
CD3
NBEAL2 p.T1454fs
WT1 p.R353fs
FLT3-ITD
UBTF-TD
D
UBTF-TD
FLT3-ITD
WT1 p.R375fs
1.9%
cells: 20
UBTF-TD
FLT3-ITD
98.1%
cells: 1051
Therapy
UBTF-TD
FLT3-ITD
WT1 p.R353fs
19.3%
cells: 125
UBTF-TD
FLT3-ITD
WT1 p.R353fs
NBEAL2 p.T1454fs
80.7%
cells: 524

Figure 3

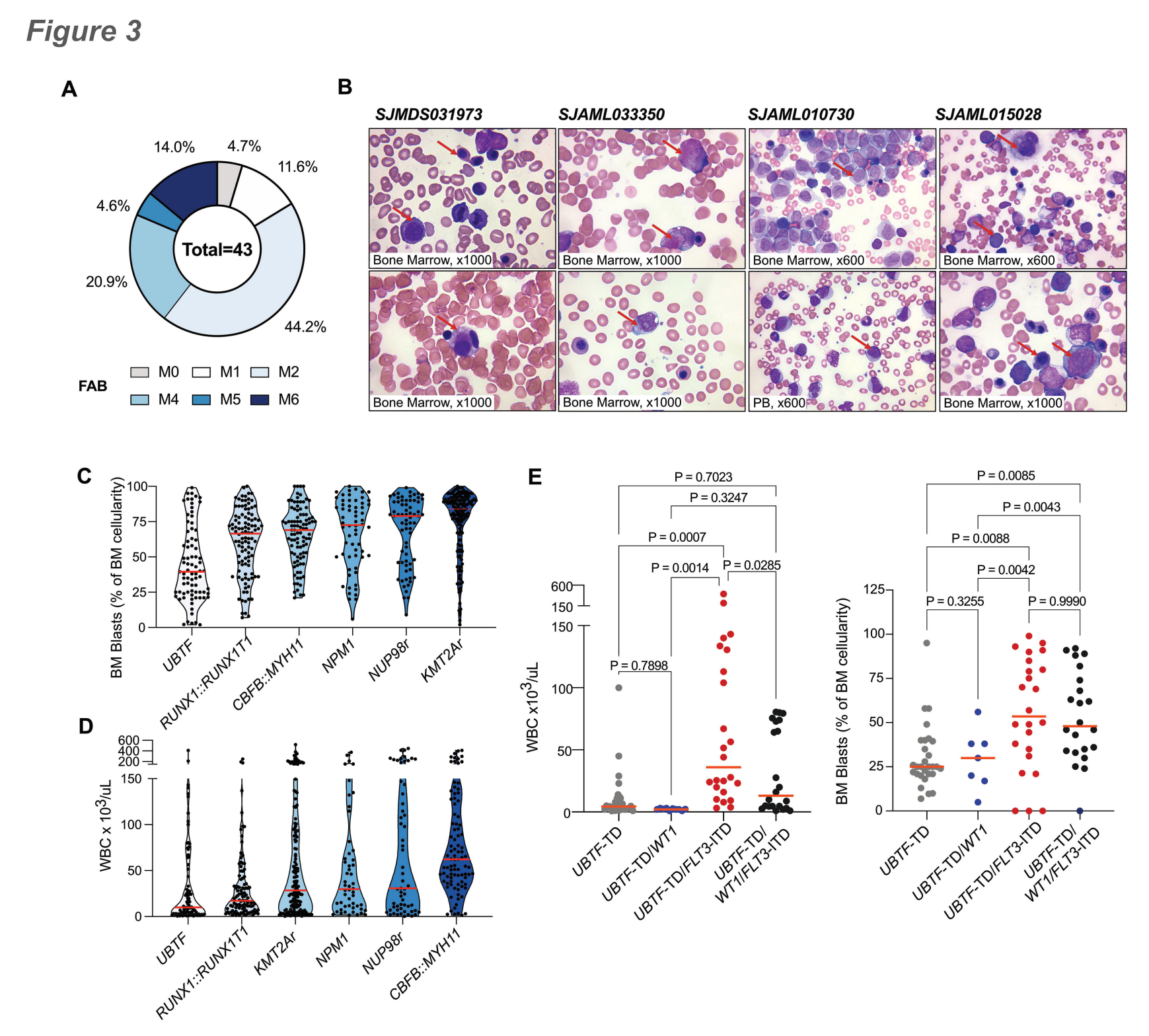
A
14.0%
4.7%
11.6%
4.6%
Total=43
20.9%
44.2%
FAB
M0
M1
M2
M4
M5
M6
B
SJMDS031973
SJAML033350
SJAML010730
SJAML015028
Bone Marrow, x1000
Bone Marrow, x1000
Bone Marrow, x600
Bone Marrow, x600
Bone Marrow, x1000
Bone Marrow, x1000
PB, x600
Bone Marrow, x1000
C
BM Blasts (% of BM cellularity)
100
75
50
25
0
UBTF
RUNX1::RUNX1T1
CBFB::MYH11
NPM1
NUP98r
KMT2Ar
D
WBC x 10^3/uL
600
400
200
150
100
50
0
UBTF
RUNX1::RUNX1T1
KMT2Ar
NPM1
NUP98r
CBFB::MYH11
E
WBC x10^3/uL
600
150
150
100
50
0
P = 0.7023
P = 0.3247
P = 0.0007
P = 0.0014
P = 0.0285
P = 0.7898
UBTF-TD
UBTF-TD/WT1
UBTF-TD/FLT3-ITD
UBTF-TD/
WT1/FLT3-ITD
BM Blasts (% of BM cellularity)
125
100
75
50
25
0
P = 0.0085
P = 0.0043
P = 0.0088
P = 0.0042
P = 0.3255
P = 0.9990
UBTF-TD
UBTF-TD/WT1
UBTF-TD/FLT3-ITD
UBTF-TD/
WT1/FLT3-ITD

Figure 4

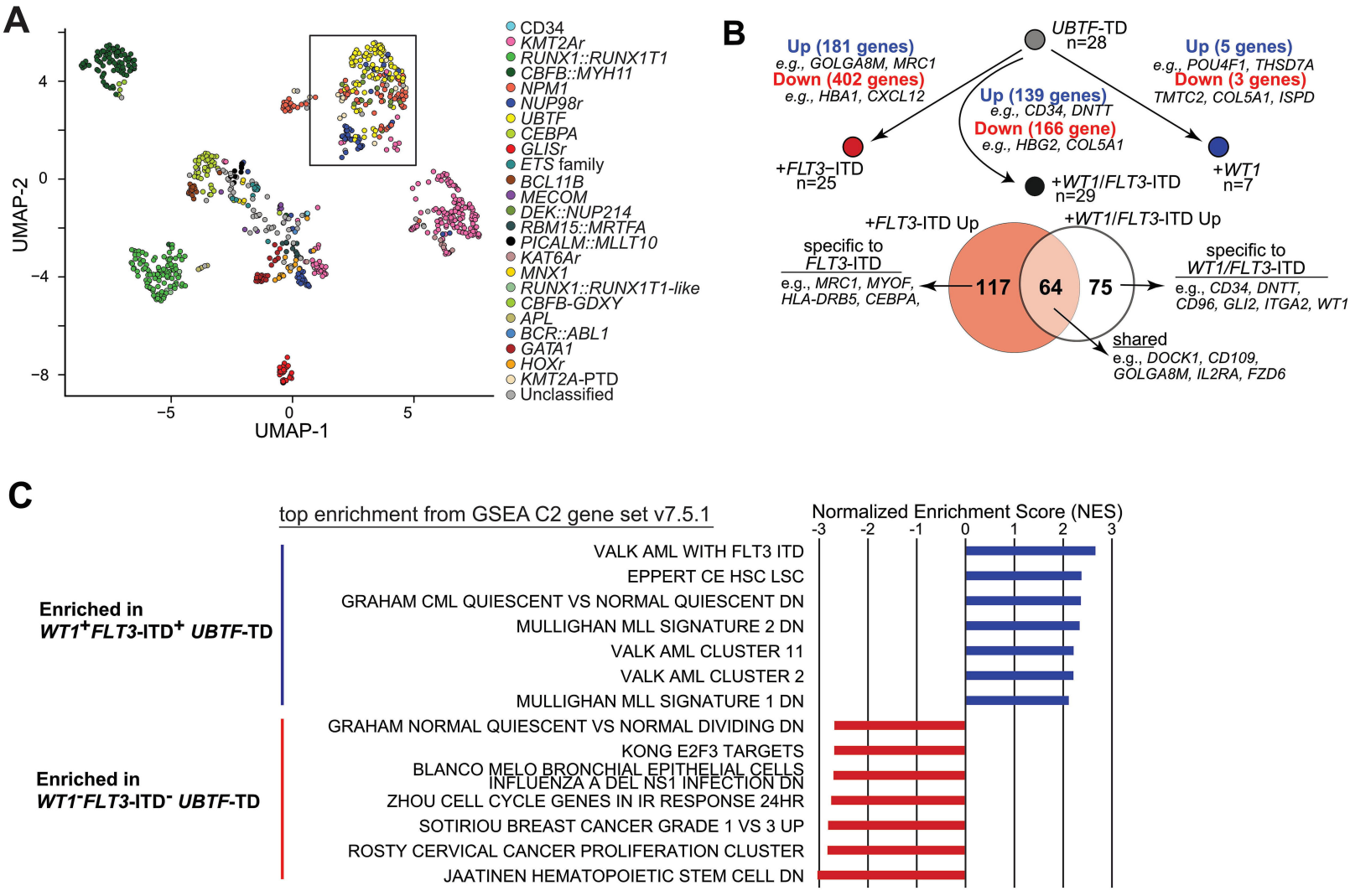
A
UMAP-2
UMAP-1
4
0
−4
−8
−5
0
5
CD34
KMT2Ar
RUNX1::RUNX1T1
CBFB::MYH11
NPM1
NUP98r
UBTF
CEBPA
GLISr
ETS family
BCL11B
MECOM
DEK::NUP214
RBM15::MRTFA
PICALM::MLLT10
KAT6Ar
MNX1
RUNX1::RUNX1T1-like
CBFB-GDXY
APL
BCR::ABL1
GATA1
HOXr
KMT2A-PTD
Unclassified
B
UBTF-TD
n=28
Up (181 genes)
e.g., GOLGA8M, MRC1
Down (402 genes)
e.g., HBA1, CXCL12
Up (139 genes)
e.g., CD34, DNTT
Down (166 gene)
e.g., HBG2, COL5A1
Up (5 genes)
e.g., POU4F1, THSD7A
Down (3 genes)
TMTC2, COL5A1, ISPD
+FLT3−ITD
n=25
+WT1/FLT3-ITD
n=29
+WT1
n=7
+FLT3-ITD Up
+WT1/FLT3-ITD Up
specific to
FLT3-ITD
e.g., MRC1, MYOF,
HLA-DRB5, CEBPA,
117
64
75
specific to
WT1/FLT3-ITD
e.g., CD34, DNTT,
CD96, GLI2, ITGA2, WT1
shared
e.g., DOCK1, CD109,
GOLGA8M, IL2RA, FZD6
C
top enrichment from GSEA C2 gene set v7.5.1
Normalized Enrichment Score (NES)
-3
-2
-1
0
1
2
3
Enriched in
WT1+FLT3-ITD+ UBTF-TD
VALK AML WITH FLT3 ITD
EPPERT CE HSC LSC
GRAHAM CML QUIESCENT VS NORMAL QUIESCENT DN
MULLIGHAN MLL SIGNATURE 2 DN
VALK AML CLUSTER 11
VALK AML CLUSTER 2
MULLIGHAN MLL SIGNATURE 1 DN
Enriched in
WT1-FLT3-ITD- UBTF-TD
GRAHAM NORMAL QUIESCENT VS NORMAL DIVIDING DN
KONG E2F3 TARGETS
BLANCO MELO BRONCHIAL EPITHELIAL CELLS
INFLUENZA A DEL NS1 INFECTION DN
ZHOU CELL CYCLE GENES IN IR RESPONSE 24HR
SOTIRIOU BREAST CANCER GRADE 1 VS 3 UP
ROSTY CERVICAL CANCER PROLIFERATION CLUSTER
JAATINEN HEMATOPOIETIC STEM CELL DN

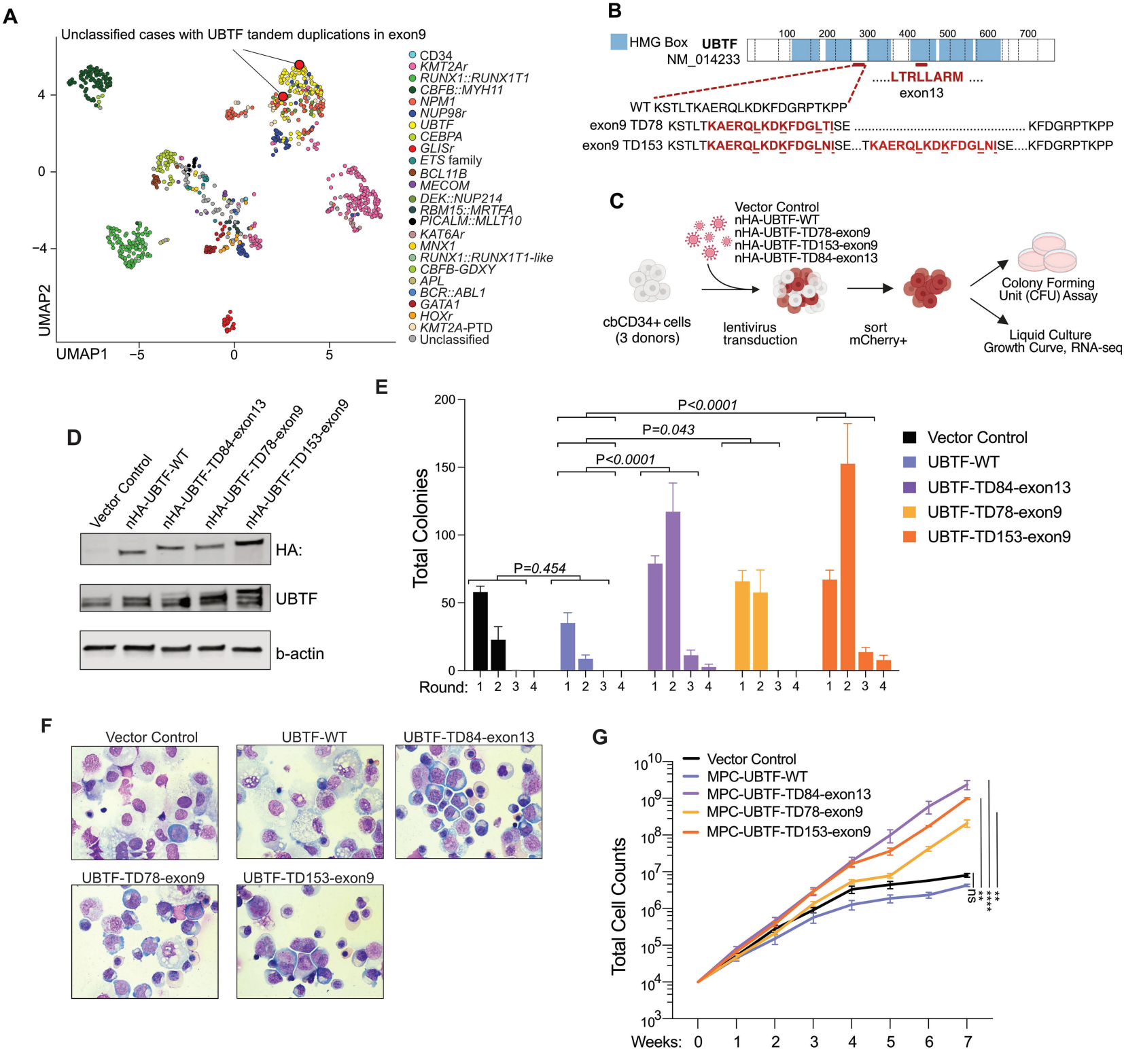
A
Unclassified cases with UBTF tandem duplications in exon9
UMAP2
UMAP1
CD34
KMT2Ar
RUNX1::RUNX1T1
CBFB::MYH11
NPM1
NUP98r
UBTF
CEBPA
GLISr
ETS family
BCL11B
MECOM
DEK::NUP214
RBM15::MRTFA
PICALM::MLLT10
KAT6Ar
MNX1
RUNX1::RUNX1T1-like
CBFB-GDXY
APL
BCR::ABL1
GATA1
HOXr
KMT2A-PTD
Unclassified
B
HMG Box
UBTF
NM_014233
LTRLLARM
exon13
WT KSTLTKAERQLKDKFDGRPTKPP
exon9 TD78 KSTLTKAERQLKDKFDGLTISE ..... KFDGRPTKPP
exon9 TD153 KSTLTKAERQLKDKFDGLNISE...TKAERQLKDKFDGLNISE....KFDGRPTKPP
C
Vector Control
nHA-UBTF-WT
nHA-UBTF-TD78-exon9
nHA-UBTF-TD153-exon9
nHA-UBTF-TD84-exon13
cbCD34+ cells
(3 donors)
lentivirus
transduction
sort
mCherry+
Colony Forming
Unit (CFU) Assay
Liquid Culture
Growth Curve, RNA-seq
D
Vector Control
nHA-UBTF-WT
nHA-UBTF-TD84-exon13
nHA-UBTF-TD78-exon9
nHA-UBTF-TD153-exon9
HA:
UBTF
b-actin
E
Total Colonies
P<0.0001
P=0.043
P<0.0001
P=0.454
Round:
Vector Control
UBTF-WT
UBTF-TD84-exon13
UBTF-TD78-exon9
UBTF-TD153-exon9
F
Vector Control
UBTF-WT
UBTF-TD84-exon13
UBTF-TD78-exon9
UBTF-TD153-exon9
G
Total Cell Counts
Weeks:
Vector Control
MPC-UBTF-WT
MPC-UBTF-TD84-exon13
MPC-UBTF-TD78-exon9
MPC-UBTF-TD153-exon9
ns
**
****
**

Supplemental Excel Table Legend		
Table Number	**File Name**	**Description**
Table 1	Supplemental_Table_1_Data_Availibility	Data availability table
Table 2	Supplemental_Table_2_Mission.Bio.Panel	Mission Bio amplicon panel
Table 3	Supplemental_Table_3_Molecular Characteristics	Molecular characteristics of 97 UBTF-TD cases
Table 4	Supplemental_Table_4_MissionBioData_Table	Mission Bio resulting SNV calls
Table 5	Supplemental_Table_5_Merged_Clinical Data	Merged clinical data of UBTF-TD cases
Table 6	Supplemental_Table_6_SNV_Calls	SNV calls used for available UBTF-TD cases

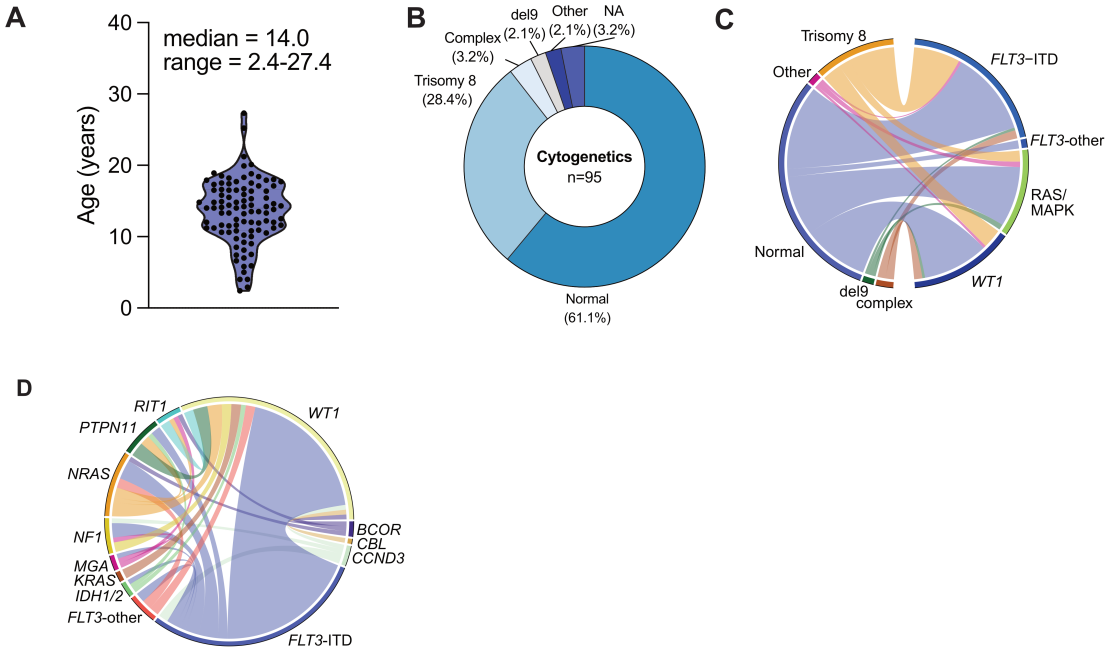

Supplemental Figure 1. Molecular and clinical characteristics of *UBTF*-TD myeloid neoplasms. **A.** Age distribution for 95 cases of myeloid neoplasms harboring UBTF-*TD* alterations in years. The median and range are shown as well. **B**. Distribution of cytogenetic changes among *UBTF*-TD cases. **C**. Ribbon plot depicting association of cytogenetics with mutations common in *UBTF*-TD myeloid neoplasms. Genes coding for proteins involved in RAS/MAPK pathway are grouped together (*NF1, PTPN11, NRAS, KRAS, RIT1, CBL)*. All other mutations in *FLT3* not classified as ITD were grouped into *FLT3*-other. **D.** Ribbon plot depicting the association of co-occurring mutations in the *UBTF*-TD cohort. Genes with only one occurrence were excluded.

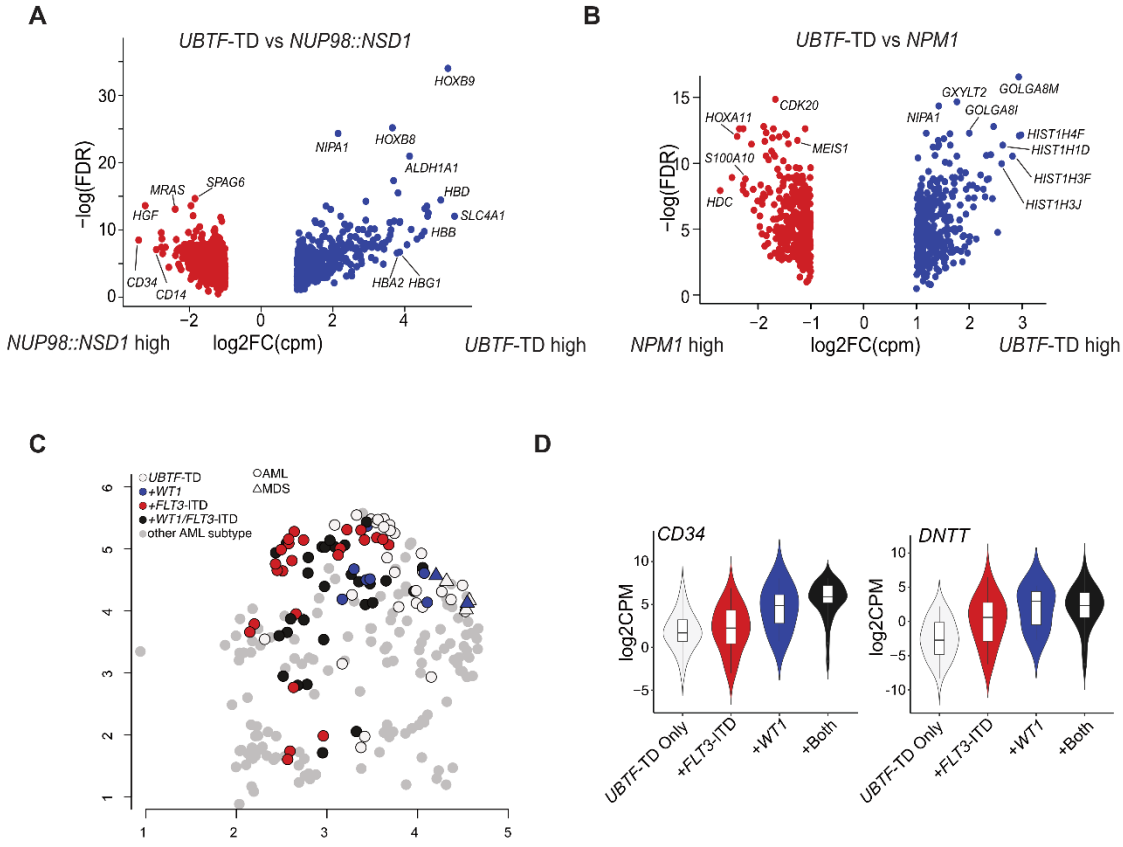

Supplemental Figure 2. Transcriptome analysis of *UBTF*-TD myeloid neoplasms. **A.** Differentially expressed genes between *UBTF*-TD AML and *NUP98::NSD1* pediatric AML. Representative genes are annotated. **B**. Differentially expressed genes between *UBTF*-TD AML and *NPM1*-mutated pediatric AML. **C.** Distribution of *UBTF*-TD cases within the cluster with *HOXA/B* dysregulation (from Figure 4A). Each data point is colored by the mutational status of *UBTF*-TD, *FLT3*-ITD, or *WT1*. MDS cases are depicted with triangles, and AML cases are with circles. **D.** Expression of *CD34* and *DNTT* with respect to *FLT3* and *WT1* mutational status. *UBTF*-TD only cases are defined as those lacking a *FLT3* or *WT1* alteration.

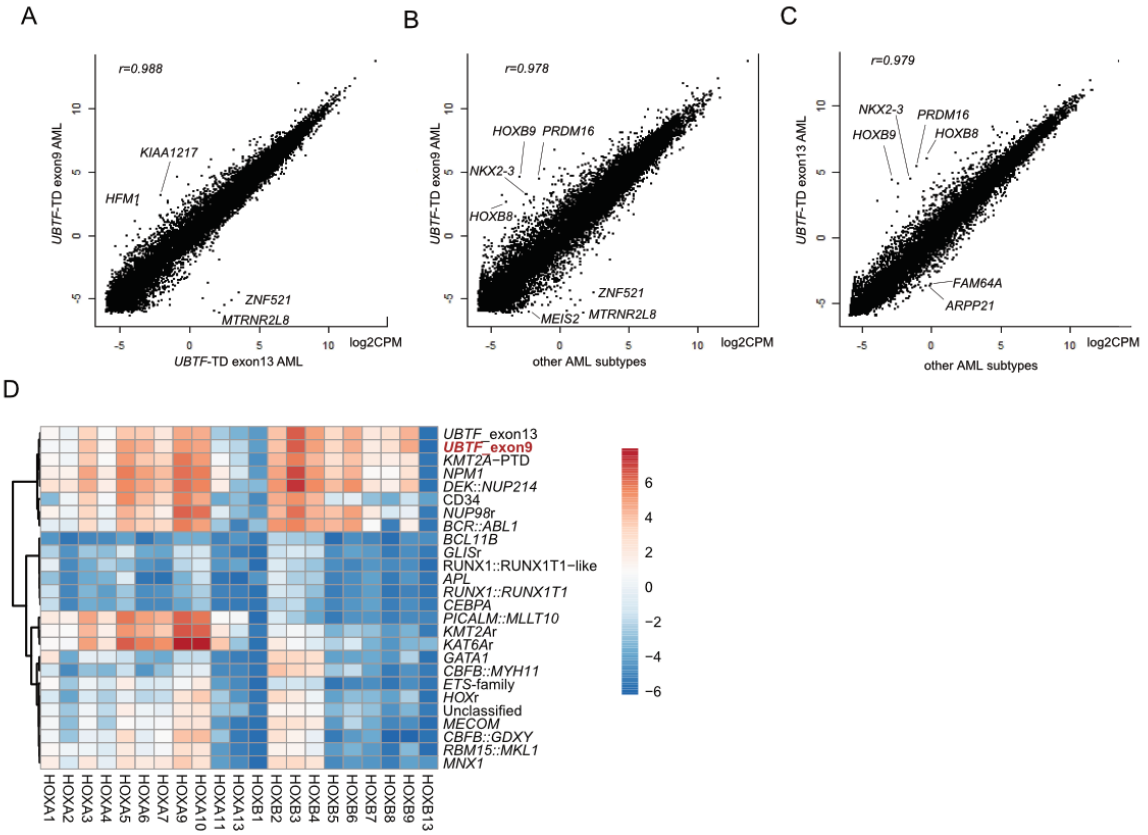

Supplemental Figure 3. *UBTF*-TD exon9 AMLs have a similar expression profile to exon13 *UBTF*-TD AMLs. **A.** Scatterplot comparing gene expressing of *UBTF*-TD exon9 AMLs to UBTF-TD exon13 AMLs. **B.** Gene expression comparison of *UBTF*-TD exon9 AMLs to other AML subtypes. **C.** Gene expression comparison of *UBTF*-TD exon13 AMLs to other AML subtypes. **D.** Heatmap depicting *HOXA/HOXB* gene expression across AML molecular categories (1).

Supplemental Methods:

RNA-sequencing and genomic profiling

As we previously performed (1), RNA reads from newly sequenced samples and from samples pulled from existing publications were mapped to the GRCh37/hg19 human genome assembly using the StrongARM pipeline (2). Chimeric fusion detection was carried out using CICERO (v0.3.0)(3). For somatic mutations calling from RNA-seq BAM files, we applied Bambino (v1.07)(4) for single nucleotide variants (SNVs) and RNAindel (v3.0.4) (5, 6) for insertions and deletions (indels), focusing on 87 predefined genes recurrently mutated in pediatric AML and MDS (1). *UBTF*-TD screening was performed as we have reported (7). For the cases with DNA capture sequencing, we called mutations as previously described (7). We also collected mutation calls with DNA data from referenced sources in **Supplemental Table 6**.

Cell Culture and Analysis of cord-blood CD34+ Cell Models

UBTF-TD cbCD34+ models were generated as previously described (7). Freshly isolated cord blood CD34+ (cbCD34+) cells were transduced with lentiviral particles from MND-PGK-mCherry constructs expressing N-terminus HA-tagged UBTF-wild-type (WT), N-terminus HA-tagged UBTF-TD84-exon13, N-Terminus HA-tagged UBTF-TD78-exon9 or N-Terminus HA-tagged UBTF-TD153-exon9. Transduced cells were sorted for mCherry positivity and expanded as previously described (7). For colony forming unit assay (CFU), 1,000 sorted cells were plated in human methocult (MethoCult™ H4435 Enriched, STEMCELL Technologies) and replated every 10 days. For every replating, 10,000 cells were plated.

Cytospins

For cytospins, 100,000 cells were washed with 1X PBS and spun onto Superfrost Plus Microscope slides (12-660-16, Fisher Scientific) at 800 rpm for 5 min.

References:

1. Umeda M, Ma J, Westover T, Ni Y, Song G, Maciaszek JL, et al. A new genomic framework to categorize pediatric acute myeloid leukemia. Nat Genet. 2024.
2. Wu G, Diaz AK, Paugh BS, Rankin SL, Ju B, Li Y, et al. The genomic landscape of diffuse intrinsic pontine glioma and pediatric non-brainstem high-grade glioma. Nat Genet. 2014;46(5):444-50.
3. Tian L, Li Y, Edmonson MN, Zhou X, Newman S, McLeod C, et al. CICERO: a versatile method for detecting complex and diverse driver fusions using cancer RNA sequencing data. Genome Biol. 2020;21(1):126.
4. Edmonson MN, Zhang J, Yan C, Finney RP, Meerzaman DM, Buetow KH. Bambino: a variant detector and alignment viewer for next-generation sequencing data in the SAM/BAM format. Bioinformatics. 2011;27(6):865-6.
5. Hagiwara K, Edmonson MN, Wheeler DA, Zhang J. indelPost: harmonizing ambiguities in simple and complex indel alignments. Bioinformatics. 2022;38(2):549-51.
6. Hagiwara K, Ding L, Edmonson MN, Rice SV, Newman S, Easton J, et al. RNAIndel: discovering somatic coding indels from tumor RNA-Seq data. Bioinformatics. 2020;36(5):1382-90.
7. Umeda M, Ma J, Huang BJ, Hagiwara K, Westover T, Abdelhamed S, et al. Integrated genomic analysis identifies UBTF tandem duplications as a recurrent lesion in pediatric acute myeloid leukemia. Blood Cancer Discov. 2022.